AEGC2019 Data to Discovery
Australasian Exploration Geoscience Conference
2-5 September 2019 • Perth, Western Australia
Incorporating the AIG, ASEG, PESA, and WABS

Geological investigations with high spatial resolution WV-3 satellite imagery and regional geophysics at the Haib Cu porphyry, Namibia

R. D. Hewson*
ITC University of Twente
PO Box 217, 7500AE, Netherlands
hewson001@gmail.com

E. Chinkaka
ITC University of Twente
PO Box 217, 7500AE, Netherlands
echinkaka@must.ac.mw

M. van der Meijde
ITC University of Twente
PO Box 217, 7500AE, Netherlands
m.vandermeijde@utwente.nl

B. Baugh
DigitalGlobe Inc.
Westminster
Colorado, USA
bill.baugh@digitalglobe.com

N. Titus
6 Aviation Rd
Namibian Geological Survey
Windhoek, Namibia
Nortin.Titus@mme.gov.na

J. P. Mubita
6 Aviation Rd
Namibian Geological Survey
Windhoek, Namibia
John-Paul.Mubita@mme.gov.na

SUMMARY

Recent improvements in available multi-spectral satellite-borne shortwave infrared sensors and their spatial resolution opens up the opportunity for furthering surface mineralogy mapping. Their image interpretation can be augmented with regional geophysics, e.g. subsurface structural information via magnetics or fine tuning the interpretation of mineral chemistry using radioelement data. The new higher spatial resolution satellite WorldView-3 sensor is compared in this study with the ASTER satellite imagery over the Haib copper prospect in southern Namibia using published geology and airborne hyperspectral imagery control.

The results show an improvement using higher spatial resolution combined with improvements in SWIR imagery for the mapping of different AlOH clays, potentially related phyllic and argillic alteration that may be associated with structurally controlled alteration and mineralisation.

Key words: Haib, WorldView-3, ASTER, radiometrics, argillic mineralisation.

INTRODUCTION

There has been considerable interest by the exploration and geoscience research community with the new DigitalGlobe multi-spectral WorldView-3 (WV-3) sensor since its launch in August, 2014, (Kruse et al., 2015). However there have been few exploration case studies to compare the capabilities of WV-3 with ASTER (Advanced Spaceborne Thermal Emission Reflection Radiometer). This study examines both ASTER and WV-3 results, and examples of the opportunities to integrate WV-3 imagery with regional geophysical data, over the Haib Cu-porphyry prospect in southern Namibia.

ASTER has been a steady workhorse for remote sensing geologists with over seven full years of archived 14 band visible (VNIR)-shortwave (SWIR) and thermal (TIR) infrared imagery at 15, 30 and 90 metres resolution, collected between 2000 and 2007 (Abrams et al., 2015). A technical malfunction has however meant that no reliable ASTER SWIR imagery has been acquired since 2007. DigitalGlobe Inc. has improved on ASTER's VNIR-SWIR spatial resolution with their 8 band 1.2 m VNIR and 8 band 7.5 m SWIR satellite sensor. The Haib area (17° 45' - 17° 59' East, 28° 37' and 28° 44' South) in southern Namibia was chosen for its active exploration interest, good geological exposure and availability of airborne hyperspectral and geophysical data for comparison and integration.

In this particular study, compositional mineral (group) products were generated using ASTER, WV-3 and compared with well calibrated airborne 126 band 5 metre resolution hyperspectral HyMap imagery (http://www.hyvista.com/) used as a reference, together with the published geological mapping (Blignault,1972). Previous exploration mapping has also been done using the HyMap data and shown to provide useful phyllic/argillic, chlorite and other mineralised information in an ore setting with major structural controls (Teck Cominco Namibia Ltd, 2009). Image processing and data/statistical analysis between the optical data and the radiometrics was undertaken. The study showed the benefits and relevance of integrating both radiometric chemistry, aeromagnetic derived structure and the high spatial resolution WV-3 derived surface geological products.

DATA AND METHODS

Two north-south acquisition strips of VNIR and SWIR WV-3 imagery over Haib were accessed via the DigitalGlobe Foundation (http://foundation.digitalglobe.com/). Due to the off NADIR angle orientation of the sensor at the time of the SWIR acquisition, a small offset exits between the two strips. The ASTER surface reflectance crosstalk corrected product (AST_07XT) was freely accessed via the NASA/USGSLPDAAC Earthdata portal (https://search.earthdata.nasa.gov/search).

WV-3 and ASTER map products were generated using band parameter indices (e.g. Relative Band Depth) described by Cudahy (2011) and developed by Crowley et al. (1989) for mineral groups including kaolinite/argillic, AlOH, MgOH-carbonate, and ferrous iron mineral content. In addition, an AlOH mineral "composition" RGB image composite was produced for both ASTER and WV-3 using band ratios as described by Hewson et al. (2005). Image product thresholds were either adopted from the methods of Cudahy (2012) or directly derived by observations of image spectral signatures testing for specific mineral absorption features. The airborne hyperspectral HyMap reference imagery was spatially subset and resampled spectrally for ASTER and WV-3 resolutions

before being processed into an equivalent mineral product discussed previously. WV-3 and ASTER were integrated with the magnetics and radiometrics via spatial resampling to the 50 metre gridded geophysics. This enabled scatterplot analysis and statistical evaluation to be undertaken. ENVI™ and ERMapper™ (ERDAS™) software was used for this study.

RESULTS

The high spatial resolution of the WV-3 VNIR at 1.2 metres was apparent in the False colour RGB (bands 7, 5 and 3) of this detailed study (Figure 1a). The Haib prospect area is highlighted in the white box. This study area is shown in the red dashed box within the geology by Blignault (1972) where the main Haib prospect lies within the various Archaen intrusive and volcanic units (Figure 1b).

The two WV-3 acquisitions were processed using the AlOH RGB band ratio product that qualitatively maps compositional clay/sericite variation (Figure 2a). Several intrusions, dolerite dykes and porphyritic units appear to be discriminated using this WV-3 product (Figure 2a) as shown by the geological lithologies A, B, C, D, E, F, and G, listed from recent Namibian geological mapping (http://www.mme.gov.na/gsn/). The Haib area with hydrothermal altered schist/andesite ("H") and porphyry ("I") units are highlighted in Figure 2a) by a generally high AlOH content, probably related to the phyllic/argillic alteration identified by (Teck Cominco Namibia Ltd., 2009). The WV-3 product was compared favourably with the same AlOH product RGB derived from the airborne HyMap data, spectrally resampled to WV-3 (Figure 2b). Similarly, the ASTER SWIR imagery was processed for AlOH composition (Figure 2c), together with the HYMap simulated ASTER product (Figure 2d). Although there were some similarities with Figures 2a) and b) results, the ASTER RGB product showed poorer spatial resolution and also spurious anomalies (red areas – higher band5/band6), as highlighted within the magenta circles (Figure 2c) that do not appear within the resampled ASTER simulated HyMap reference product (Figure 2d). The likely explanation is the issue of SWIR Crosstalk (Hewson and Cudahy, 2011) that is associated with topographically shadowed dark areas, highlighted in the SRTM DEM (magenta, Figure 2e), artificially illuminated to simulate the solar angle at the time of ASTER acquisition (9/3/2003). The Ternary K-Th-U image shows some radioelement variation for the different intrusions however it appears to discriminate less than the SWIR imagery, although in part possibly related to the coarser 50 m gridded resolution (Figure 2f).

An integrated RGB composite image of WV-3 derived AlOH content, Ferrous iron bearing MgOH mineral content and the TMI RTP 1VD for the same area shows the complementary nature of these optical and geophysical information (Figure 2g). In particular, the amphibolite/hornblende units (Figure 1b) and pervasive greenschist altered chlorite bearing units, appear to be highlighted by the WV-3 Ferrous Iron MgOH product (green), distinct from the AlOH bearing mineralogy associated with the intrusions and areas of alteration (Figure 2g). The incorporation of the 1VD magnetics also highlights the dolerite dykes ("F") and the dyke bearing Vioolsdrif Alkali Granite ("G"). A WV-3 kaolinite/argillic index product was derived via targeting (e.g. masking) areas of higher WV-3 AlOH content and showed distinct anomalies associated with the Ramansdrif Granite ("B") and the Haib altered areas ("H" and "I") (Figure 2h). This product has the potential to also highlight alteration areas of higher crystalline kaolinite forms (e.g. dickite) and advanced argillic minerals such as alunite (Cudahy, 2012).

An example of evaluating the relationship between potassium content and WV-3 AlOH content was examined (Figure 3a and b). Three concentration ranges of K were chosen to observe the possible AlOH variation. For example, kaolinite doesn't contain potassium however present within illite, muscovite and the advanced argillic mineral, alunite. It is feasible that the Leucogranite (Figure 1b and Figure 3a - "C") contains orthoclase or another higher K-bearing feldspar, in the western part of the study area. Other K-bearing AlOH minerals appear to be highlighted within the Tsams Meta Rhyolite ("D" – Figure 2h)) and associated E-W to NW oriented shear zone. The Haib prospect area appears to also include higher K bearing AlOH within the "I" unit (Vioolsdrif Quartz Feldspar Porphyry) shown in Figure 3a.

Recent structural interpretative work by Chinkaka (2019), using an automated line extracting algorithm on first vertical derivative reduced-to-the-pole magnetic data, highlighted several structures related to the older NE-SW Orange River and younger NW-SE Namaqua Orogenic events (Figure 3c). Some of these coincided favourably with several linear AlOH bearing anomalies derived from WV-3 simulated HyMap data (Figure 3c, Figure 2b). Identifying associations of alteration mineralogy with aeromagnetic interpreted structures is potentially important given the structurally controlled nature of the Haib Cu-porphyry deposit (Teck Cominco Namibia Ltd, 2009).

CONCLUSIONS

The results to date of processing satellite-borne WV-3 imagery over the Haib prospect showed the benefits of using higher spatial resolution WV-3, which compared favourably with simulations from airborne HyMap hyperspectral imagery. Simple RGB band ratios produced qualitative AlOH compositional information that compared favourably with recent geological mapping of intrusives and volcanics, without the presence of residual Crosstalk SWIR false anomalies that can be apparent with the equivalent ASTER product. Ternary radiometric imagery showed limited discrimination of the surface geology, however incorporating potassium radioelement concentration with SWIR derived AlOH/clay mapping enhanced mineral chemistry discrimination and possible mapping of argillic alteration. It also appeared that interpreting and integrating both magnetics and SWIR derived mineral mapping could help enhance the understanding of structurally controlled alteration and possible mineralised deposition. Further work is needed to assess and validate these results as well as evaluate the robustness of such higher spatial resolution imagery in less arid and more vegetated environments.

ACKNOWLEDGEMENTS

Our thanks go to the DigitalGlobe Foundation Inc. for providing this imagery for our research work with WorldView-3 imagery and the Geological Surveys of Namibia for providing us with the HyMap imagery, aeromagnetic data and geological mapping information. The ASTER imagery was made available via the product

distribution of the US NASA/USGS and Japan's METI organizations.

REFERENCES

Abrams, M., H. Tsu, G. Hulley, K. Iwao, D. Pieri, T. Cudahy, and J. Kargel, 2015, The Advanced Spaceborne Thermal Emission and Reflection Radiometer (ASTER) after fifteen years: Review of global products, International Journal of Applied Earth Observation and Geoinformation, 38, 292-301, doi: http://dx.doi.org/10.1016/j.jag.2015.01.013.

Blignault, H. J., 1972, Geological Map of Haib area. Geological Survey of Namibia. Windhoek.

Chinkaka, E., 2019, Integrating WorldView-3, ASTER and aeromagnetic data for lineament structural interpretation and tectonic evolution of the Haib area, Namibia" MSc Thesis, University of Twente.

Crowley, J.K., Brickey, D.W. and Rowan, L.C., 1989, Airborne imaging spectrometer data of the Ruby Mountains, Montana: mineral discrimination using relative absorption band depth images. Remote Sensing of Environment, vol. 29, no. 2, 121–134.

Cudahy, T.J., 2012, Australian ASTER Geoscience Product Notes, Version 1, 7th August, 2012 – CSIR0, ePublish No. EP-30-07-12-44, 2012.

Kruse, F. A., Baugh, W. M. and Perry, S. L., 2015, Validation of DigitalGlobe WorldView-3 Earth imaging satellite shortwave infrared bands for mineral mapping, Journal of Applied Remote Sensing, 9(1), 96044., https://doi.org/10.1117/1.JRS.9.096044

Hewson, R.D. and Cudahy, T.J., 2011, Issues affecting geological mapping with ASTER data: a case study of the Mt Fitton area, South Australia. In: Ramachandran, B., ed. Land Remote Sensing and Global Environmental Change: NASA s Earth Observing System and the Science of ASTER and MODIS: Applications in ASTER, Springer-Verlag, New York, ISBN: 978-1-4419-6748-0.

Teck Cominco Namibia Ltd, 2009, Renewal Report: Exclusive Prospecting Licence 3140. Retrieved from https://www.deepsouthresources.com/wp-content/uploads/Haib_NI43-101_May-3-2016_FINAL.pdf

Hewson R.D., Cudahy T., Mizuhiko S., Ueda K., and Mauger A.J., 2005, Seamless geological map generation using ASTER in the Broken Hill-Curnamona Province of Australia. Remote Sensing of Environment, 99:159–172.

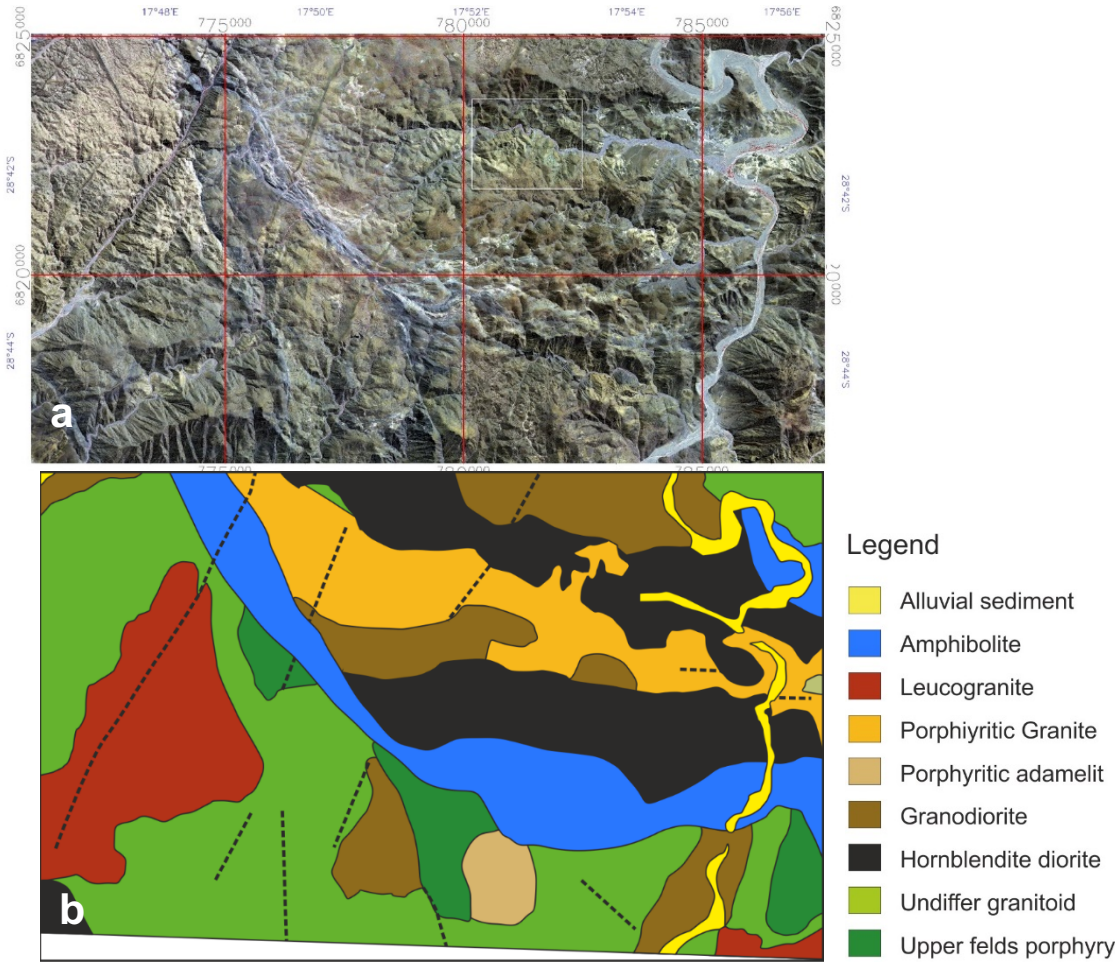

Figure 1. a) World View-3 RGB of bands 7, 5, 3 of the study area, with the Haib Prospect area within the white box; b) The geology of Blignault (1972) within the same areal extents, as shown in (a).

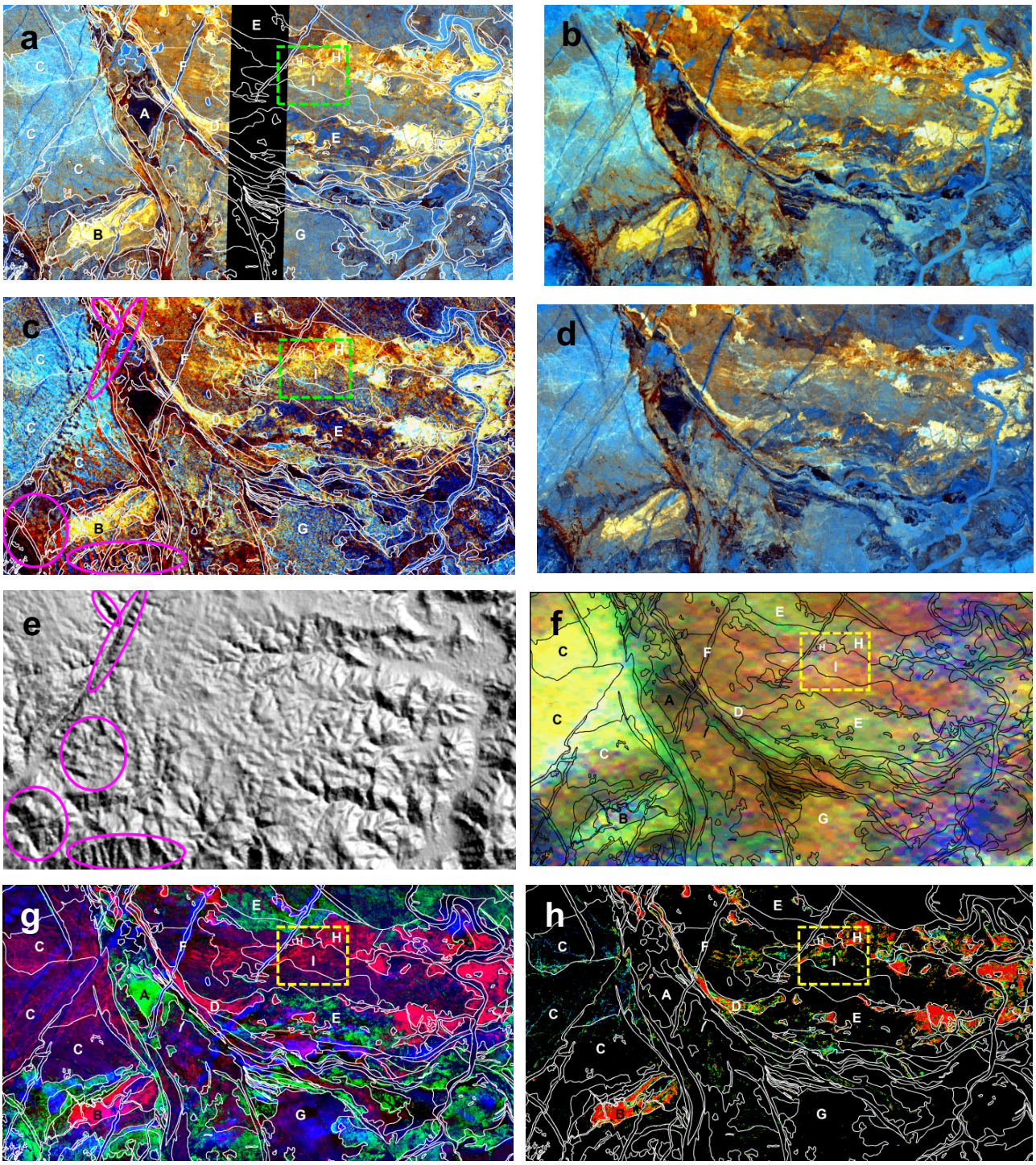

Figure 2 a) WV-3 AlOH RGB product; b) HyMap simulated WV-3 AlOH RGB product; c) ASTER AlOH RGB product with anomalous B5/B6 AlOH areas circled (magenta); d) HyMap simulated ASTER AlOH RGB product; e) SRTM DEM artificial shaded (56° azimuth, 52° elevation), with areas of anomalous B5/B6 AlOH (magenta); f) radiometric ternary RGB of K (1-5%), Th (5-35 ppm) and U (0-30 ppm); g) RGB composite: WV-3 AlOH content, WV-3 Ferrous bearing MgOH content, TMI RTP 1VD; h) WV-3 kaolinite/argillic content, within areas of higher WV-3 AlOH content (>2.15). Haib general Cu porphyry prospect area in dashed yellow box. Provisional lithological boundary vectors overlain in white line (Courtesy of Namibian Geological Survey) with descriptions:
A : Tsams Andesite; B : Ramansdrif Granite; C : Gaarseep Granite; D : Tsams Metarhyolite; E : Porphyritic Tsams Andesite; F : Namibian Dolerite Intrusives; G : Vioolsdrif Alkali Granite (including aplite dykes); H : Tsams Chlorite Schist / hydrothermal altered andesite; I : Vioolsdrif Quartz Feldspar Porphyry.

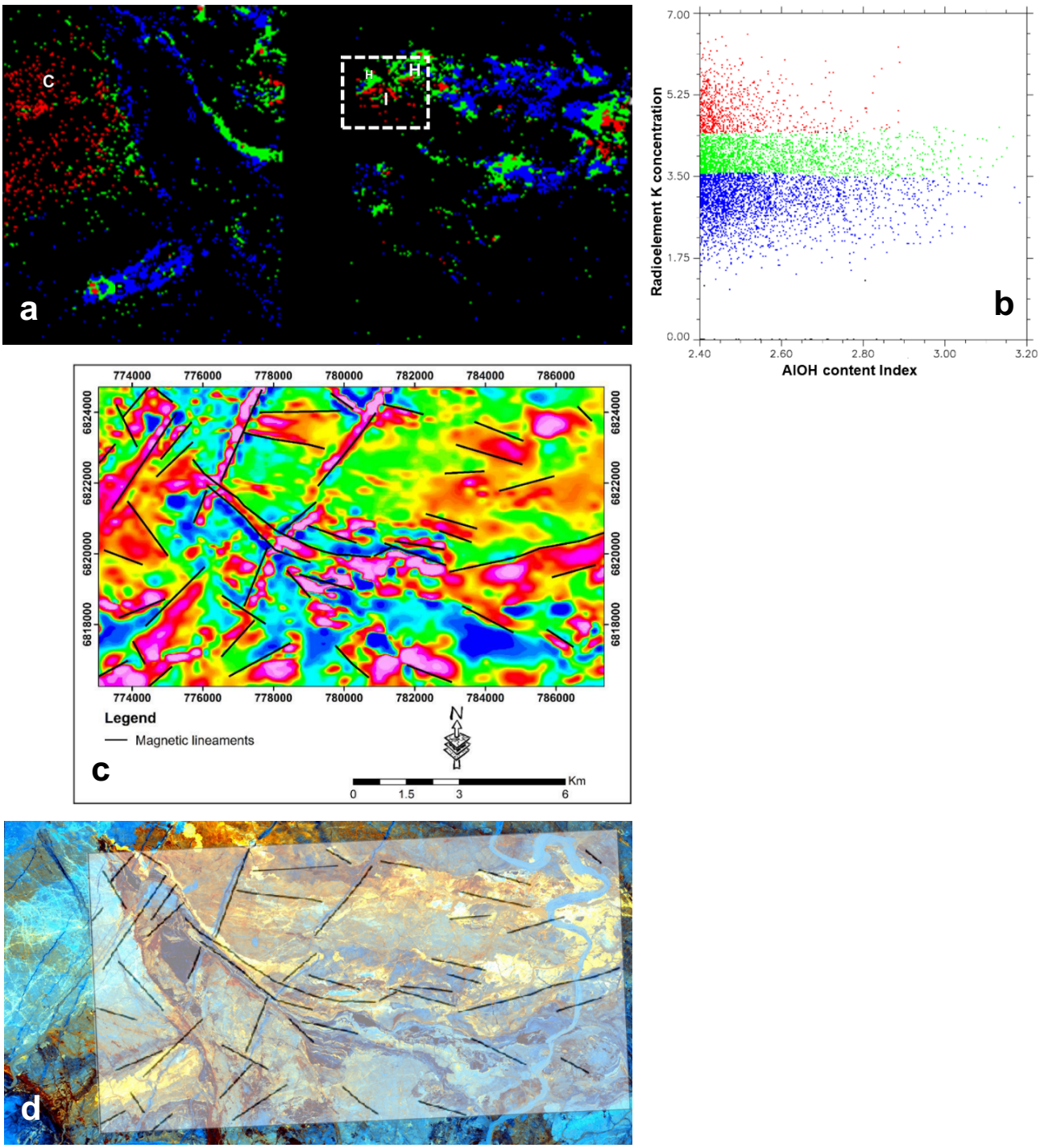

Figure 3. a) WV-3 AlOH content product threshold for >2.4 and classified based on radioelement K concentration as classified in b) scatterplot for decreasing K from red (>4.4 %), green and blue (<3.5%), Note the higher K bearing AlOH content (red) within the Haib prospect area (dashed white); c) TMI RTP 1VD interpreted lineaments (Chinkaka, 2019) overlain onto the WV-3 simulated HyMap AlOH RGB (Figure 2b) product, showing the partial alignment of dykes/faults and clay/AlOH bearing units.